Plant Methods

RESEARCH

Open Access

Attomolar electrochemical direct and sandwich immunoassays for the ultrasensitive detection of tomato brown rugose fruit virus

Negin Rezaei[1], Ahmad Moshaii[2*], Mohammad Reza Safarnejad[3], Reza H. Sajedi[4], Mahsa Rahmanipour[2] and Masoud Shams-Bakhsh[1]

Abstract

Tomato brown rugose fruit virus (TBRFV; *Tobamovirus fructirugosum*) is a highly virulent tobamovirus that has emerged as a major global threat to tomato and pepper crops over the past decade. Early and ultra-sensitive detection of TBRFV is critical for effective disease management and the mitigation of agricultural losses. In this study, a highly sensitive electrochemical immunosensor was developed based on both direct and sandwich immunoassays for the detection of TBRFV. The assay employs TBRFV-CP-IgG and TBRFV-CP-IgG^{HRP} antibodies, with the latter conjugated to horseradish peroxidase (HRP). The immunoassays were assembled on a nanoporous gold electrode, providing an enhanced electroactive surface for efficient antigen capture and signal amplification. Electrochemical characterization confirmed the successful immobilization of TBRFV-CP-IgG, its specific interaction with the recombinant coat protein of TBRFV (rp-CP-TBRFV), the subsequent binding of TBRFV-CP-IgG^{HRP} as the detection antibody, and the formation of the complete sandwich complex. The assays achieved linear detection ranges of 10–10^5 fg/mL. The direct assay yielded a limit of detection (LoD) of 1.14 fg/mL (65.14 aM), while the sandwich assay, enhanced by enzymatic amplification, achieved 1.06 fg/mL (60.57 aM). The direct assay's simplicity suits rapid diagnostics, whereas the sandwich assay's superior sensitivity is ideal for low-concentration samples. Electrochemical characterization confirmed specific antigen capture and signal amplification. The biosensor demonstrated high specificity, distinguishing TBRFV from other viruses, and detected TBRFV in leaf and seed extracts, offering a promising platform for agricultural biosecurity.

Keywords TBRFV, Electrochemical immunosensor, Horseradish peroxidase, Sandwich immunoassays

*Correspondence:
Ahmad Moshaii
moshaii@modares.ac.ir
[1]Plant Pathology Department, Faculty of Agriculture, Tarbiat Modares University (TMU), Tehran, Iran
[2]Department of Physics, Tarbiat Modares University, P.O Box 14115-175, Tehran, Iran
[3]Department of Plant Viruses, Iranian Research Institute of Plant Protection, Agricultural research, education and extension organization (AREEO), Tehran, Iran
[4]Department of Biochemistry, Faculty of Biological Sciences, Tarbiat Modares University, Tehran, Iran

Introduction

The tomato brown rugose fruit virus (TBRFV; *Tobamovirus fructirugosum*) is an emerging tobamovirus with a positive-sense single-stranded RNA genome containing four open reading frames (ORFs). It belongs to the virgaviridae family and the tobamovirus genus. Over the past decade, TBRFV has rapidly spread worldwide, reaching pandemic levels with a high prevalence rate. It was first reported in Jordan in 2015 [1] and has since been detected across all continents [2, 3]. The virus primarily infects solanaceae species, particularly tomatoes and peppers, posing a severe threat to global crop production. Notably, resistance genes such as Tm (in tomatoes) and L (in peppers), which confer resistance against related viruses, have proven ineffective against TBRFV [4, 5].

TBRFV is primarily transmitted through direct contact between infected and healthy plants, contaminated seeds, agricultural tools, equipment, and human-mediated transfer (via contaminated hands or clothing). This high transmissibility facilitates long-distance spread [6]. Additionally, some insect vectors may contribute to its dissemination. The hallmark symptoms of TBRFV infection include mosaic patterns, leaf narrowing, dark green blistering on leaves, and brown, wrinkled spots on fruits, significantly reducing the marketability of affected crops [1, 7]. Given its high environmental stability and extensive transmission potential, strict hygiene protocols, equipment disinfection, and the use of virus-free seeds are crucial for containment. Studies indicate that TBRFV can reduce crop yields by 15–55%, even in tomato plants carrying the *Tm-22* resistance gene [8]. Thus, the development of highly sensitive and precise diagnostic methods is essential for effective virus detection and management.

Among various diagnostic approaches, electrochemical immunosensors have attracted significant attention due to their high sensitivity, low detection limits, and cost-effectiveness [9–12]. These biosensors function by immobilizing specific antibodies onto a sensitive transducer surface, where they selectively interact with the target antigen, generating a measurable electrochemical response. This allows for rapid, highly specific detection of viral antigens, even at ultra-low concentrations, in complex biological samples [13, 14]. Studies have shown that integrating nanostructured materials into electrochemical biosensors—such as nanocomposites [15], graphene [16], silver nanoparticles [17], and gold nanostructures [18] enhances the effective electroactive surface area, facilitates charge transfer, and significantly improves sensor sensitivity. Among these, gold nanostructures are particularly advantageous due to their high electrical conductivity, biocompatibility, and resistance to oxidation [19].

Electrochemical biosensors can be designed in a sandwich assay format, incorporating a secondary antibody conjugated to an electroactive enzyme, such as horseradish peroxidase (HRP). Upon exposure to 3,3′,5,5′-tetramethylbenzidine (TMB) in the presence of H_2O_2, HRP catalyzes redox reactions, leading to the electrochemical detection of the target analyte [20]. Previous studies have demonstrated that enzyme-labeled antibodies in electrochemical biosensors enhance signal amplification, increase sensitivity, and improve detection performance [21–24]. This sandwich electrochemical immunosensor approach has been successfully applied in detecting various pathogens and biomarkers, including breast cancer patients [25], exosomes [26], Enterovirus 71 [20], carcinoembryonic antigen (CEA) [9, 27], and the CA15-3 tumor marker [28]. Additionally, similar biosensing platforms have been utilized for detecting plant viruses, including cucumber mosaic virus (CMV) [29], rice tungro disease (RTD) [30], and citrus tristeza virus (CTV) [31].

The present study aims to develop a highly sensitive and specific electrochemical immunosensing platform for the ultrasensitive detection of TBRFV using both direct and sandwich-format immunoassays. The biosensor employs electrodes modified with nanoporous gold nanostructures [32]. The immunosensing system utilizes TBRFV-CP-IgG and TBRFV-CP-IgG^{HRP} antibodies, along with the recombinant TBRFV coat protein antigen (rp-CP-TBRFV). Electrochemical characterization was performed using cyclic voltammetry (CV), electrochemical impedance spectroscopy (EIS), and differential pulse voltammetry (DPV) in the presence of the TMB/H_2O_2 substrate. The developed biosensor exhibited a wide linear detection range from 10 to 10^5 fg/mL, with an ultra-low detection limit of 1.14 fg/mL (65.14 aM), demonstrating high specificity and excellent reproducibility. Furthermore, the sensor successfully detected TBRFV in leaf tissue extracts (up to 1:256 dilution) and seed extracts (up to 1:2 dilution). This study introduces a highly promising electrochemical biosensing strategy for TBRFV detection, providing a powerful tool for plant biosecurity and effective virus management, ultimately mitigating the widespread damage caused by this emerging pathogen.

Materials and methods

Reagents and materials

High-purity gold (99.99%) and silver (99.99%) metals, fluorine-doped tin oxide (FTO) substrates (15 Ω/sq, 0.8 × 1.25 cm², 2 mm thickness), and phosphate-buffered saline (PBS, pH 7.4) were used as fundamental materials. Chemicals including mercaptoacetic acid (MAA), 1-ethyl-3-(3-dimethylaminopropyl) carbodiimide (EDC), and N-hydroxysuccinimide (NHS) were procured from Sigma-Aldrich. Additional reagents included gelatin, ethanol (99.9%), pure acetone (99.98%,

Merck), and recombinant TBRFV coat protein (rp-CP-TBRFV) expressed in *Escherichia coli* [33]. The lysis buffer comprised lysozyme, NaH_2PO_4 (50 mM), NaCl (300 mM), and imidazole (10 mM). The TBRFV-CP-IgG antibody was prepared as previously described by Rezaei et al. [33], and subsequently conjugated with horseradish peroxidase (HRP) (Merck, Germany) using the periodate method [33]. Electrochemical measurements were conducted using potassium chloride (KCl), potassium ferricyanide ($K_3[Fe(CN)_6]$), potassium ferrocyanide ($K_4[Fe(CN)_6]$), and deionized water (DI water). All reagents were used without further purification.

Electrochemical instrumentation

Electrochemical measurements, including CV, EIS, and DPV, were carried out using the Origalysis potentiostat system (ElectroChem SAS, France). The system employed a three-electrode configuration: an Ag/AgCl reference electrode, a gold plate counter electrode, and a nanoporous gold-modified working electrode.

Expression and purification of rp-CP-TBRFV

The recombinant TBRFV coat protein was expressed and purified as follows: The CP gene, fused with a His-tag, was cloned into the pET-28a (+) bacterial expression vector and transformed into *E. coli* BL21. Expression was induced in a 1 L culture at 28 °C using 0.5 mM isopropyl-β-D-thiogalactopyranoside (IPTG) for 3 h under continuous shaking at 180 rpm. The bacterial pellet was resuspended in lysis buffer (50 mM NaH_2PO_4, 300 mM NaCl, 10 mM imidazole, pH 8.0) containing 1 mg/mL lysozyme, followed by eight cycles of sonication (30-second pulses at 182 W with 30-second intervals). Purification was conducted under native conditions using immobilized metal ion affinity chromatography (IMAC) per the manufacturer's instructions (Qiagen, Netherlands) [33]. SDS-PAGE analysis confirmed the purity and expression of recombinant TBRFV-CP, revealing a distinct band at approximately 23 kDa [33].

Fabrication of the sensing electrode

Electrode preparation and surface modification followed the protocol described by Yarjou et al. [32]. Initially, FTO electrodes were thoroughly cleaned with acetone, ethanol (99.9%), and DI water, followed by ultrasonication for 15 min and subsequent drying in an oven. A thin layer of 5 nm silver and 5 nm gold was sequentially deposited onto the FTO electrodes using physical vapor deposition (PVD) under a vacuum of 1×10^{-6} Torr. The deposition rate was maintained at 0.1 nm/s, with layer thickness monitored via a quartz crystal microbalance. Nanoporous Ag-Au alloy nanostructures were obtained by thermally annealing the electrodes at 550 °C for 2 h. The dealloying process was conducted by immersing the annealed electrodes in 65% nitric acid at room temperature for 15 min, followed by extensive rinsing with DI water. SEM images of a representative nanoporous gold electrode, along with its EDS quantitative analysis, are presented in Fig. S1 of the Supplementary Information. In addition, the reproducibility of the sensor was evaluated by measuring the peak current values using cyclic voltammetry (CV) across five independently fabricated bare electrodes, which demonstrated consistent performance with minimal variation (Fig. S2, Supplementary Information). Long-term stability was assessed by monitoring the electrochemical response of a representative electrode over a four-week period, revealing sustained activity and reliable functionality throughout the duration of storage (Fig. S2, Supplementary Information).

Biofunctionalization of the sensor

For biofunctionalization, the gold surface was initially treated with 50 µL of 14 mmol/L MAA solution for 2 h at room temperature, followed by ethanol (65%) washing. Carboxyl group activation was achieved using 50 µL of 50 mM EDC/NHS (1:1) in PBS (pH 4.5) for 1 h at room temperature. Next, 50 µL of 10 µg/mL TBRFV-CP-IgG was immobilized onto the activated electrode and incubated overnight at 4 °C to ensure stable antibody attachment. To establish the sandwich assay, blocking was performed using 50 µL of 20 mg/mL gelatin in PBS for 45 min. Various concentrations of rp-CP-TBRFV were incubated separately on individual working electrodes for 45 min at 4 °C. Subsequently, 50 µL of 0.42 µg/mL TBRFV-CP-IgG^{HRP} was added and incubated for 1 h at 4 °C [21]. Between each step, electrodes were rinsed thoroughly with PBS (pH 7.4). To prevent photochemical degradation of MAA thiol groups, all functionalization steps were conducted in a dark environment.

The selection of sensing experimental parameters, including the concentration of the primary antibody (TBRFV-CP-IgG), incubation time, and incubation period, was guided by the methodology reported in Yarjoo et al. [32], and these conditions were subsequently evaluated and validated for compatibility with the current sensing assay. The concentration of the secondary antibody (TBRFV-CP-IgG^{HRP}) was selected based on the findings of Rezaei et al. [33], where this concentration was identified as the minimum level capable of reliably detecting both the coat protein (CP) and intact viral particles in real samples using the ELISA method.

Electrochemical measurements

Electrochemical characterization was performed in a 20 mL electrolyte solution containing 2.5 mM $[Fe(CN)_6]^{3/4}$ and 0.1 M KCl, using an Ag/AgCl reference electrode. Each measurement was conducted in triplicate. CV was recorded from −300 mV to 450 mV at a scan rate of 50

mV/s. EIS was measured across a frequency range of 0.1 Hz to 10^5 Hz (Zre vs. Zim at 160 mV vs. Ag/AgCl reference). DPV measurements were recorded within a range of 10 µA to 100 µA [32]. All electrochemical measurements were carried out at room temperature. The final electrochemical detection was performed following the formation of the sandwich complex in the presence of TMB (15 µM) and H_2O_2 (20 µM) in 0.1 M KCl [34].

Performance and selectivity of the immunosensor

To evaluate the immunosensor's performance, a calibration curve was generated, and the limit of detection (LoD) was determined using serial dilutions of rp-CP-TBRFV in PBS (pH 7.4), ranging from 0 to 10^5 fg/mL. Furthermore, the sensor's selectivity was assessed in the presence of potential interfering agents from real samples. This included serial dilutions of infected leaf tissue extract (1:64 to 1:512), infected seed extract (1:2 to 1:4), and leaf extracts containing tobacco mosaic virus (*Tobamovirus tabaci*; TMV), cucumber mosaic virus (*Cucumovirus cucumovirus*; CMV), and tomato yellow leaf curl virus (*Begomovirus coheni*; TYLCV). Extracts from virus-free leaf and seed samples served as negative controls.

Extraction of plant sap

Plant sap was extracted by grinding 0.1 g of tomato leaf tissues in the presence of liquid nitrogen using a mortar and pestle, followed by suspending the homogenate in 2000 µL of phosphate-buffered saline (PBS; pH 6.5) [35]. For seed extract preparation, 1 gram of tomato seeds was incubated overnight at 4 °C in 10 mL of phosphate buffer. Subsequently, the seed extract was separated from the soaked seeds by centrifugation at 5000 rpm for 5 min. Both healthy and virus-infected sap samples were stored at -20 °C until further use [36].

Results and discussion

The detection of TBRFV with the developed immunosensor system can be carried out using two sensing approaches. The first is direct measurement of the viral coat protein and the second is the sandwich-assay of the protein based on an HRP-labeled antibody as the enzyme and TMB/H_2O_2 as the substrate. For both sensing approaches, the modified electrode surface was functionalized using MAA, EDC, and NHS to activate covalent bonding [32, 37] and ensure stable immobilization of the TBRFV-CP-IgG antibody. The immunosensor characteristics were assessed using CV, EIS, and DPV.

Prior to the immobilization of TBRFV-CP-IgG, the electrode surface was characterized in its bare state, without sensing elements. The immobilization process involved TBRFV-CP-IgG attachment, blocking with gelatin to fill any unoccupied surface sites [38–40], the addition of rp-CP-TBRFV as the antigen, and TBRFV-CP-IgG^{HRP} as the enzyme-labeled antibody. Finally, to evaluate the immunocomplex interaction, the enzymatic substrate TMB/H_2O_2 was introduced. Electrochemical measurements were performed after each step of immunocomplex formation and substrate addition and the results have been shown in Fig. 1.

Figure 1a presents CV measurements of the biosensor at various stages of fabrication and surface functionalization. The analysis focuses on six key stages: the bare electrode, antibody immobilization, gelatin blocking, viral antigen binding, secondary antibody attachment, and enzymatic substrate reaction. The CV of the bare electrode (Porous Au) shows a high anodic peak current of 705 µA, indicating robust electron transfer at the pristine nanoporous gold surface. This high conductivity reflects the electrode's clean, unmodified state, where redox-active species in the electrolyte (e.g., $[Fe(CN)_6]^{3-/4-}$) can freely access the surface, facilitating efficient oxidation and reduction reactions.

Upon immobilizing TBRFV-specific antibodies at a concentration of 10 µg/mL, the anodic peak current decreases sharply to 560 µA. This reduction arises because the antibody layer introduces steric hindrance and insulating properties, obstructing electron transfer between the electrode and the electrolyte. The drop in current confirms successful antibody attachment, as the biomolecules block the electrode's active sites, reducing its electrochemical activity. After blocking unoccupied surface sites with gelatin, the current decreases further (to 541 µA). Gelatin acts as a biocompatible barrier, preventing nonspecific binding of unwanted molecules. This step is critical for enhancing selectivity, as it ensures that subsequent interactions are specific to the target antigen. The introduction of the viral antigen (rp-CP-TBRFV) at 1 pg/mL causes the current to decline further (to 520 µA). This reduction occurs because the antigen binds to the immobilized antibodies, forming the first layer of the immunocomplex. This interaction increases the surface resistance, indicating successful capture of the target analyte. Adding the HRP-labeled secondary antibody (TBRFV-CP-IgG^{HRP}) at 0.42 µg/mL results in a further drop in current (to 513 µA). The secondary antibody binds to the antigen, creating a thicker immunocomplex layer. This amplifies steric hindrance and insulating effects, reducing electrochemical activity.

Upon exposure to the TMB/H_2O_2 substrate, the anodic peak current increases dramatically to 627 µA, nearly restoring it to the initial bare electrode value (705 µA). This recovery occurs because HRP catalyzes the oxidation of 3,3',5,5'-tetramethylbenzidine (TMB) by hydrogen peroxide (H_2O_2), generating a soluble redox-active product (TMB). This product shuttles electrons to the electrode, bypassing the insulating immunocomplex layers.

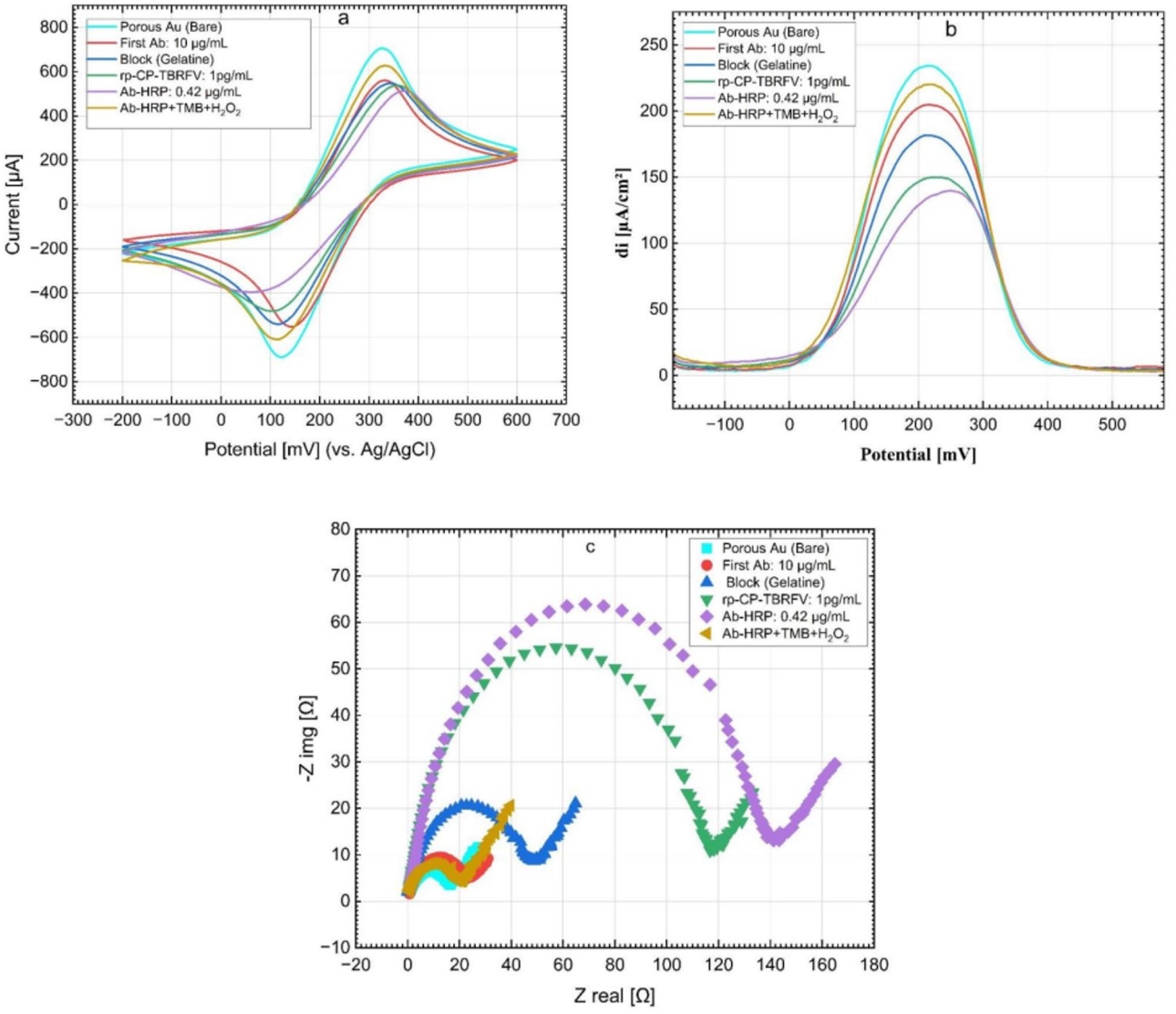

Fig. 1 Electrochemical response graphs, including CV (**a**) at a scan rate of 50 mV/**s**, DPV (**b**), and EIS (**c**), corresponding to different stages of the biosensor formation. These stages include the porous electrode, antibody immobilization, blocking with gelatin, addition of the viral surface protein (rp-CP-TBRFV), HRP-labeled secondary antibody, and finally, exposure to the enzymatic substrate (TMB/H_2O_2)

The sharp increase in current validates the enzymatic amplification strategy, which is pivotal for achieving ultra-low detection limits (e.g., 1.06 fg/mL).

To validate the specificity of the immunosensor response, a series of control experiments were performed and are presented in Fig. S3 in Supplementary Information. These controls include measurements in the absence of the capture antibody, the target antigen, and the HRP-conjugated secondary antibody. In all cases, the lack of significant electrochemical signal confirmed that the sensor response is not due to nonspecific adsorption or background interactions, but rather arises specifically from the targeted antigen–antibody recognition events.

Figure 1b presents DPV measurements, which provide higher sensitivity to subtle changes in electrochemical activity compared to CV. The results track the biosensor's response across its fabrication and functionalization stages. The initial peak current density for the bare electrode is 234 µA/cm², reflecting unimpeded electron transfer at the pristine electrode surface. After antibody attachment, the current density decreases to 205 µA/cm². This reduction is attributed to the insulating properties of the antibody layer, which blocks direct electron transfer between the electrode and the redox probe ($[Fe(CN)_6]^{3-/4-}$). The introduction of the viral antigen (1 pg/mL) causes a further decline to 150 µA/cm². This drop confirms the formation of the antigen-antibody immunocomplex, which increases surface resistance and restricts electron transfer.

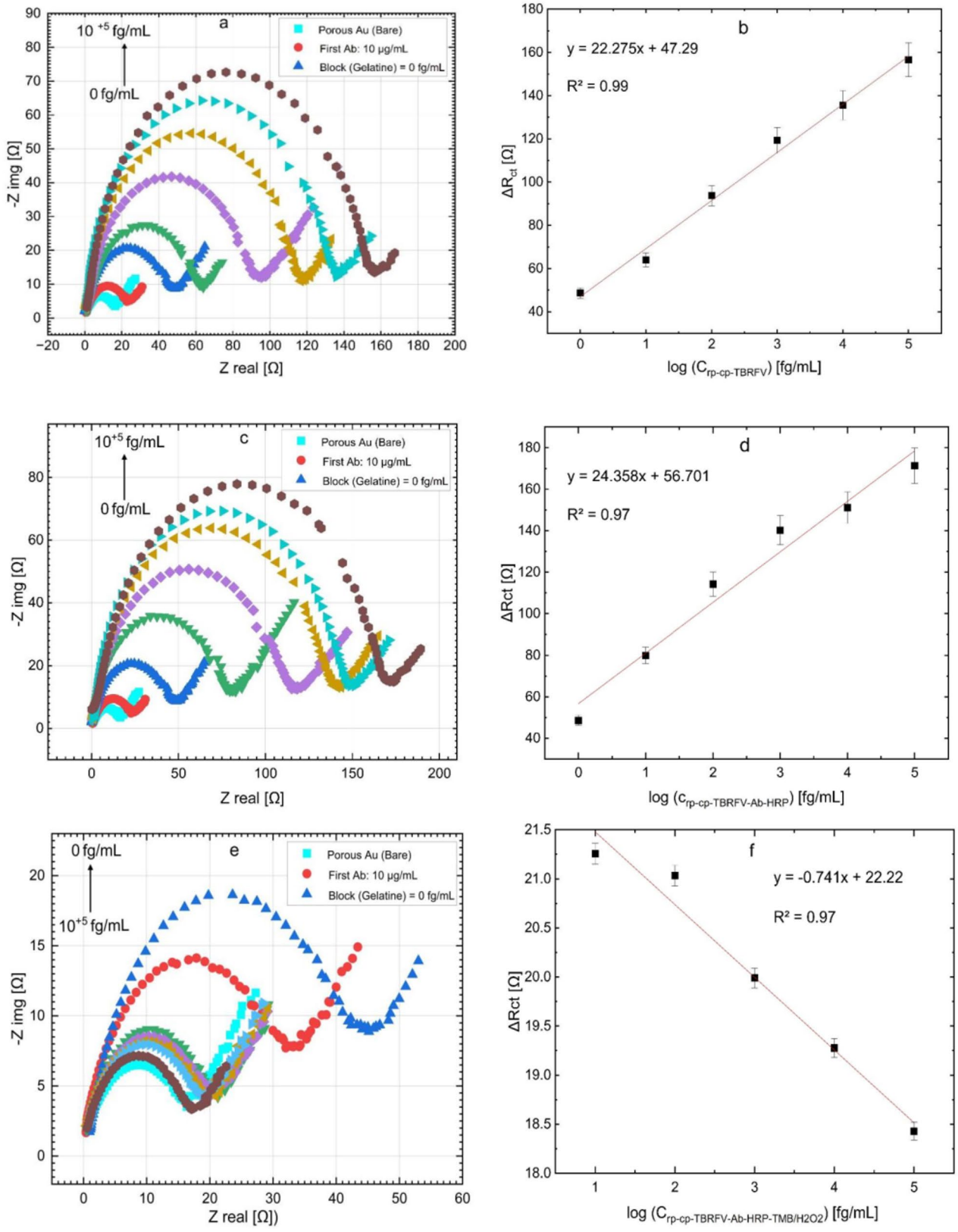

Fig. 2 (See legend on next page.)

(See figure on previous page.)

Fig. 2 The electrochemical characterization for the detection of TBRFV using different biosensing strategies. (**a**) EIS response for direct immunosensing at various concentrations of rp-CP-TBRFV. (**b**) Corresponding calibration curve demonstrating a linear relationship between ΔR_{ct} and the logarithm of rp-CP-TBRFV concentration. (**c**) EIS response for the sandwich immunoassay incorporating the HRP-labeled secondary antibody TBRFV-CP-IgG^{HRP}. (**d**) Calibration curve showing enhanced signal amplification in the sandwich assay. (**e**) EIS response after enzymatic reaction with TMB/H_2O_2, demonstrating a decrease in charge transfer resistance. (**f**) Calibration curve illustrating the recovery of electrochemical activity following enzymatic catalysis. The results confirm that the sandwich immunoassay improves sensitivity compared to direct immunosensing, and the enzymatic reaction further enhances detection performance, making the developed biosensor a highly effective tool for TBRFV detection

After immobilizing the HRP-labeled secondary antibody (TBRFV-CP-IgG^{HRP}), the current density decreases to 140 μA/cm². The thicker immunocomplex layer amplifies steric hindrance and insulation, further reducing electrochemical activity. Upon exposure to the substrate, enzymatic reaction with TMB/H_2O_2 occurs and the current density surges to 220 μA/cm², nearing the bare electrode's value (234 μA/cm²). The DPV results corroborate the CV findings, validating the enzymatic amplification strategy for enhancing sensitivity.

Figure 1c displays the EIS data, which measures charge transfer resistance (R_{ct}) at the electrode-electrolyte interface. The Nyquist plots illustrate how each functionalization step affects the interfacial resistance. These plots show the real (Z′) versus imaginary (Z″) components of impedance over a frequency range of 0.1 Hz to 100 kHz. The semicircular portion corresponds to the charge transfer resistance (R_{ct}), with its diameter directly reflecting the efficiency of electron transfer at the electrode-electrolyte interface. An increase in the semicircle diameter indicates a rise in R_{ct}, signifying hindered charge transfer due to surface modification or target binding events. The initial R_{ct} of the bare electrode is 16 Ω, indicative of a conductive surface with minimal resistance to electron transfer. The R_{ct} increases to 22 Ω after the first antibody attachment. After the gelatin blocking and antigen binding, further resistance increases are observed as gelatin and antigen layers add steric hindrance. The R_{ct} for the secondary antibody immobilization is about 141 Ω, reflecting the cumulative insulating effect of the immunocomplex layers. Post-substrate addition of TMB/H_2O_2, results in R_{ct} plummets to 20 Ω, nearly matching the bare electrode's resistance. This dramatic reduction occurs because TMB , generated by HRP-catalyzed oxidation, acts as a redox mediator, restoring efficient electron transfer.

The EIS results complement the CV and DPV data, demonstrating how the biosensor's resistance dynamically responds to bio-recognition events and enzymatic reactions. This triad of electrochemical techniques collectively validates the sensor's design, enabling femtogram-level sensitivity and specificity for TBRFV detection. In addition, the trend of results in Fig. 1 aligns well with previous reports in the literature [20, 21].

Figure 2 provides a detailed electrochemical characterization of the developed immunosensor for detecting TBRFV using three distinct biosensing strategies: direct immunoassay, sandwich immunoassay, and enzymatic immunoassay. The figure is divided into six panels (a–f), each presenting EIS responses and corresponding calibration curves across a concentration range of 10 to 10^5 fg/mL of the coat protein rp-CP-TBRFV.

The EIS response for direct immunoassay are shown in Fig. 2a and b assessing the sensor's performance in detecting rp-CP-TBRFV through direct antigen-antibody interactions. The ΔR_{ct} increases progressively with antigen concentration. At 0 fg/mL (negative control), ΔR_{ct} ≈ 22 Ω (baseline). At 10^5 fg/mL, ΔR_{ct} rises to ~141Ω. A linear relationship is observed between ΔR_{ct} and the logarithm of rp-CP-TBRFV concentration. The regression coefficient (R^2) is 0.99, indicating strong linearity and reliability. Calculating LoD using the formula LoD = S/3.3σ, where σ is the standard deviation of blank signals ($n = 3$ replicates), and S is calibration curve slope, results in the LoD of the direct immunoassay as low as 1.14 fg/mL (equivalent to 65.14 aM).

To enhance sensitivity, a sandwich immunoassay format is employed, as shown in Fig. 2c. The dual-antibody approach amplifies the signal, as evidenced by a steeper increase in ΔR_{ct} compared to the direct assay. At 10^5 fg/mL, ΔR_{ct} reaches ~210 Ω, reflecting the cumulative insulating effect of the antigen and secondary antibody layers. The calibration curve in Fig. 2d demonstrates a linear relationship (R^2 = 0.97) between ΔR_{ct} and antigen concentration, with a calculated LoD of 1.06 fg/mL. This result demonstrates superior sensitivity due to the sandwich format, which enhances antigen-antibody interactions and the signal output.

The enzymatic amplification strategy is showcased in Fig. 2e. After forming the sandwich complex, the TMB/H_2O_2 substrate is introduced. Consequently, ΔR_{ct} decreases dramatically, reverting from ~210 Ω (post-secondary antibody) to ~20 Ω (near baseline) at 10^5 fg/mL. This reversal confirms the efficacy of enzymatic amplification in overcoming steric hindrance. Figure 2f quantifies this response, showing a linear decrease in ΔR_{ct} with increasing antigen concentration (R^2 = 0.97).

While the signal recovery demonstrates the effectiveness of the enzymatic amplification strategy, it also introduces some limitations in discrimination clarity. The less pronounced discrimination observed in Fig. 2e-f, compared to the direct EIS measurements in Fig. 2a-d, can be attributed to the nature of the enzymatic amplification strategy employed. In the TMB/H_2O_2 system, the

redox mediator (oxidized TMB) enhances electron transfer at the electrode surface, thereby reducing the overall impedance. While this approach increases signal magnitude and helps restore conductivity, it also compresses the ΔR_{ct} values across different antigen concentrations, making differences between analyte levels appear less distinct. In contrast, the direct and sandwich EIS measurements (Fig. 2a–d) reflect cumulative interfacial resistance changes due to immunocomplex formation at each stage.

Figure 3 Real-sample detection and selectivity of the electrochemical immunosensor for TBRFV. (a) Electrochemical response curves for TBRFV detection in serially diluted infected leaf extracts (1:64 to 1:512), demonstrating concentration-dependent signal attenuation via sandwich immunoassay. (b) Calibration curve for leaf extract dilutions, showing a linear relationship (R^2 = 0.99) between charge transfer resistance (ΔR_{ct}) and logarithmic dilution factor. (c) Selectivity assessment: The immunosensor exhibits strong specificity for TBRFV in infected leaf (1:256 dilution) and seed extracts (1:2 dilution), with negligible cross-reactivity (< 10% background signal) against non-target viruses (TMV, CMV, TYLCV) or virus-free controls. Results validate the sensor's femtogram-level sensitivity, field-deployable utility, and robustness in complex agricultural matrices.

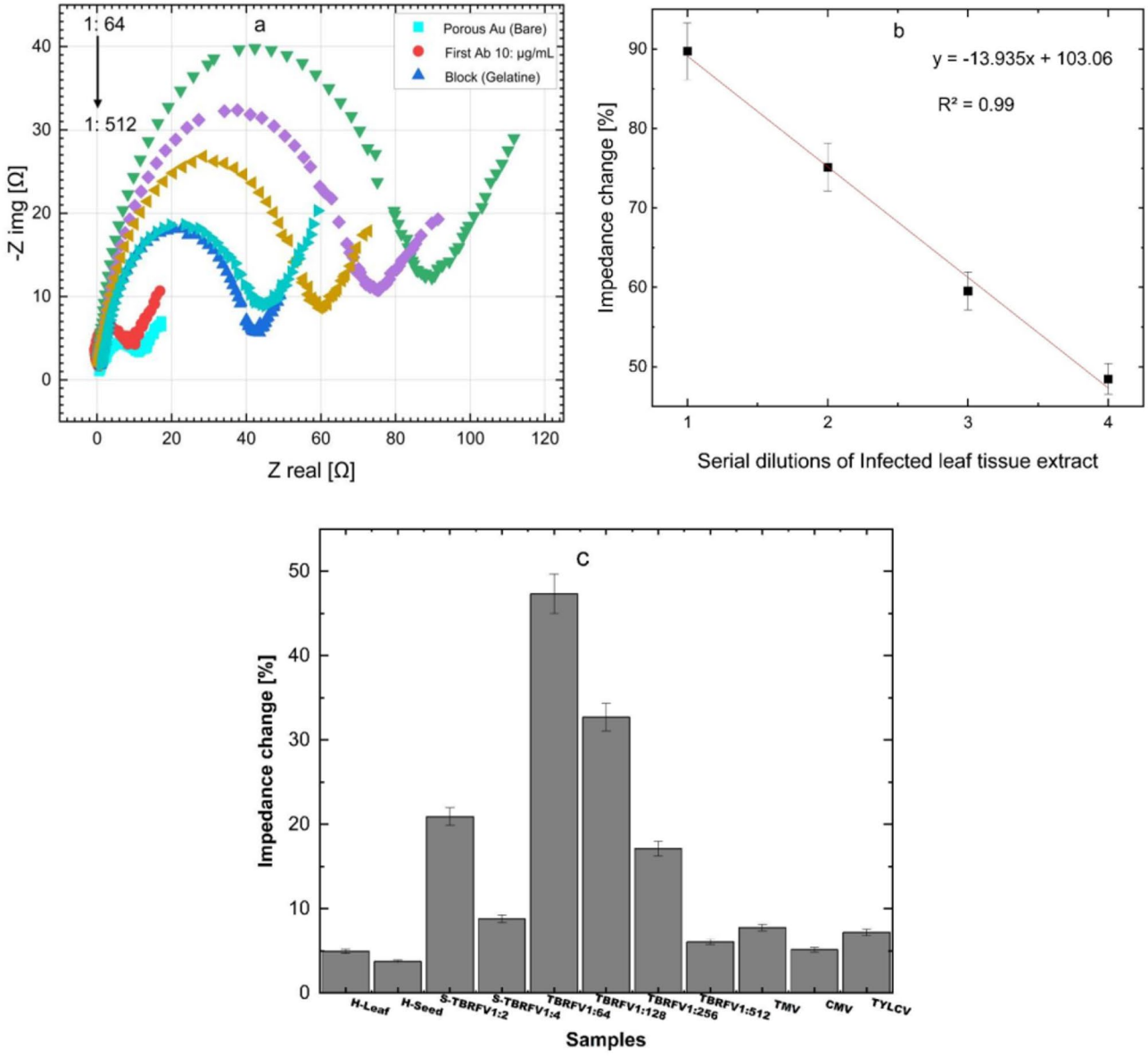

Fig. 3 demonstrates the practical applicability, sensitivity, and selectivity of the developed electrochemical immunosensor for detecting TBRFV in real agricultural samples. The figure comprises three panels (**a**, **b**, **c**), showcasing the sensor's performance in infected leaf and seed extracts, calibration curves, and cross-reactivity tests against non-target viruses

Table 1 Comparison of analytical performance metrics for various electrochemical sandwich immunoassays reported in the literature, including linear detection ranges, lod, and detection methods. The table encompasses biosensors targeting plant viruses (e.g., cucumber mosaic virus and citrus Tristeza virus) as well as human and animal pathogens (e.g., enterovirus 71 and carcinoembryonic antigen), highlighting the superior sensitivity and performance of the developed TBRFV immunosensor

Biosensor substrate	Detection method	Linear range	LoD	Refs
ITO/ AuNPs/ MUA/ EDC-NHS/ mAb/ EV71/ mAb-HRP	CA*	0.1– 600 ng/mL	0.01 ng/mL	[20]
Anti-CEA/Ce-MoF@HA/Ag-HRP/GCE	CA EIS	0.001– 80 ng/mL	0.2 pg/mL	[9]
CS-NG/GCE /Au@Ag/HRP-anti-CEA	DPV	0.0001– 100 ng/mL	0.05 pg/mL	[27]
SPCE/ Anti- CMV/ CMV/ Anti-CMV-HRP	CA	0.1–1.3 mg/mL	0.1 mg/mL	[29]
CP- CTV/ Ab_2/ MB/ HRP	DPV	1.95– 10.0×10^3 fg/mL	0.3 fg/mL	[31]
MNP–HBsAb/HBsAg/HBsAb–HRP	CV	0.001– 0.015 ng/ mL	0.9 pg/mL	[41]
Ab1/CEA/(DNA/(ZMPs-HRP-Ab2)n	CV	0.008–200 ng/mL	5 pg/mL	[42]
AuC-HRP-anti-AFP/AFP-anti-AFP-O-MB-AuNPs/GCE	DPV	0.005–20 ng/mL	1.5 pg/mL	[43]
Au nano-porous/MAA/EDC-NHS/TBRFV-CP-IgG/Gelatin/rp-CP-TBRFV/ TBRFV-CP-IgG^{HRP}	EIS CV DPV	10–10^5 fg/ mL	Direct assay: 1.14 fg/mL Sandwich assay: 1.06 fg/mL	This work

*: Chronoamperometry

Figure 3a presents the electrochemical response curves for a dilution series of TBRFV-infected leaf extracts, ranging from 1:64 to 1:512 dilutions. The immunosensor employs the sandwich immunoassay format, where TBRFV-specific antibodies (TBRFV-CP-IgG and TBRFV-CP-IgG^{HRP}) capture the virus particle in the samples. The results reveal a concentration-dependent decrease in current intensities, with detectable signals even at the highest dilution (1:256). This indicates the sensor's ability to identify ultra-low viral concentrations in complex biological matrices. The progressive signal attenuation correlates with reduced antigen availability at higher dilutions, validating the assay's dynamic range.

Figure 3b illustrates the corresponding calibration curve for the leaf extract dilution series. The plot exhibits a linear relationship between the electrochemical signal (ΔR_{ct}) and the logarithm of the dilution factor, with a regression coefficient (R^2) of 0.99. This strong linearity confirms the sensor's reliability and reproducibility in quantifying TBRFV across varying concentrations.

Figure 3c evaluates the immunosensor's selectivity by testing its response to TBRFV-infected leaf and seed extracts versus negative controls and samples containing non-target viruses (TMV, CMV, TYLCV). The results show that in the leaf extracts, TBRFV is detectable at dilutions up to 1:256, confirming robust performance in complex plant matrices. While in the seed extracts, the detection is achieved at 1:2 dilutions, highlighting the sensor's utility in screening infected seeds, a critical pathway for viral transmission. In addition, the sensor exhibits negligible cross-reactivity (< 10% of the TBRFV signal) with TMV, CMV, TYLCV, or virus-free samples. This specificity ensures reliable differentiation of TBRFV from phylogenetically related viruses, such as TMV (a tobamovirus genetically close to TBRFV).

To further support the analytical performance of the biosensor and its concentration-dependent response across various sensing configurations, additional CV measurements are presented in Fig. S4 of the Supplementary Information. These include CV responses for the direct and sandwich immunoassays, the post-enzymatic reaction stage, and serial dilutions of infected leaf extracts. The results reinforce the sensor's sensitivity to TBRFV and provide complementary validation to the EIS data.

Table 1 provides a comprehensive comparison of the analytical capabilities of various electrochemical sandwich immunoassays documented in the literature, highlighting the performance metrics of the developed TBRFV immunosensor in the context of existing biosensing platforms. The table illustrates the linear detection ranges, detection limits (LoD), and references for several biosensors targeting different pathogens and biomarkers, including Enterovirus 71, carcinoembryonic antigen (CEA), and plant viruses such as CMV and CTV. This comparison underscores the versatility of electrochemical biosensors in diverse fields, from medical diagnostics to agricultural biosecurity, while highlighting the superior sensitivity and performance of the developed TBRFV immunosensor. Notably, the TBRFV immunosensor developed in this study demonstrates a remarkable linear detection range from 10 to 10^5 fg/mL, with an ultra-low LoD of 1.14 fg/mL (equivalent to 65.14 aM) for the direct assay and 1.06 fg/mL (equivalent to 60.57 aM) for the sandwich assay. These values surpass the sensitivity of many previously reported biosensors, such as those for CEA (LoD of 0.2 pg/mL) and CMV (LoD of 0.1 mg/mL), underscoring the exceptional sensitivity of the proposed platform. The integration of nanoporous gold nanostructures and HRP-labeled antibodies in the sandwich assay format significantly enhances signal amplification,

enabling femtogram-level detection of TBRFV. This comparison not only validates the superior performance of the developed immunosensor but also positions it as a highly competitive tool for ultrasensitive detection of plant viruses, with potential applications in agricultural diagnostics and biosecurity.

To evaluate the developed immunosensors, we compared direct and sandwich immunoassay strategies for TBRFV detection. The direct assay involves the binding of recombinant TBRFV coat protein (rp-CP-TBRFV) to immobilized TBRFV-CP-IgG antibodies, producing an electrochemical signal via EIS, CV, and DPV. It offers a simple, reagent-efficient workflow with an assay time of ~2 h and achieves a limit of detection (LoD) of 1.14 fg/mL (65.14 aM) over a linear range of 10–105 fg/mL (R^2 = 0.99). In contrast, the sandwich assay introduces an HRP-labeled secondary antibody that binds to the captured antigen, enabling enzymatic amplification through the TMB/H_2O_2 redox reaction. This increases the assay time to ~3 h but improves sensitivity, reaching an LoD of 1.06 fg/mL (60.57 aM) with comparable linearity (R^2 = 0.97).

The sandwich assay's superior sensitivity makes it well-suited for early detection in low-concentration samples, such as highly diluted leaf extracts (1:256, Fig. 3a), and it outperforms many reported biosensors (Table 1). However, reliance on HRP and TMB/H_2O_2 introduces variability, potentially limiting reproducibility in non-laboratory environments. The direct assay, despite a slightly higher LoD, is advantageous for rapid, low-cost, field-deployable diagnostics due to its straightforward protocol. Both methods utilize the same nanoporous gold platform, ensuring consistency, and together provide complementary tools for diverse agricultural diagnostic applications.

Conclusions

In this study, we have successfully developed an ultrasensitive electrochemical immunosensor for the detection of TBRFV, leveraging both direct and sandwich immunoassay formats. The biosensor employs nanoporous gold-modified electrodes and HRP-labeled antibodies to achieve exceptional sensitivity and specificity. The electrochemical characterization, conducted through CV, EIS, and DPV, confirmed the successful immobilization of TBRFV-specific antibodies, the formation of antigen-antibody complexes, and the enzymatic amplification of the electrochemical signal.

The developed immunosensor demonstrated an ultra-low detection limit of 1.14 fg/mL (equivalent to 65.14 attomolar) for the direct assay and 1.06 fg/mL (equivalent to 60.57 aM) for the sandwich assay, which surpasses the sensitivity of conventional detection methods such as ELISA and fluorescent quantum dot-based assays. This remarkable sensitivity is attributed to the efficient signal amplification provided by the HRP-catalyzed redox reaction in the presence of the TMB/H_2O_2 substrate. The biosensor also exhibited excellent specificity, effectively distinguishing TBRFV from other closely related plant viruses, including TMV, CMV, and TYLCV. This high specificity ensures reliable detection in complex agricultural matrices, reducing the risk of false positives.

The practical applicability of the immunosensor was validated through its ability to detect TBRFV in infected leaf and seed extracts, even at extreme dilution factors (1:256 for leaf extracts and 1:2 for seed extracts). This capability is crucial for early detection and containment of TBRFV outbreaks, particularly in agricultural settings where the virus can spread rapidly through contaminated seeds, tools, and human contact. The sensor's robustness and reproducibility further underscore its potential as a reliable diagnostic tool for plant biosecurity.

The integration of nanoporous gold nanostructures into the electrode design played a pivotal role in enhancing the sensor's performance. The high surface area and excellent electrical conductivity of the nanoporous gold facilitated efficient antigen capture and signal amplification, while the biocompatibility and resistance to oxidation ensured the stability of the immunosensor over time. The use of HRP-labeled antibodies in the sandwich assay format further enhanced the sensitivity, allowing for the detection of trace amounts of TBRFV in complex samples.

This study not only presents a highly sensitive and specific method for TBRFV detection but also highlights the broader potential of electrochemical immunosensors in agricultural diagnostics. The developed platform offers a rapid, cost-effective, and field-deployable solution for the early detection of plant pathogens, which is critical for preventing widespread agricultural losses. Future work will focus on integrating this sensing platform into portable electrochemical devices, enabling real-time monitoring and on-site diagnostics in agricultural settings. This advancement could significantly enhance the ability to manage and mitigate the impact of emerging plant viruses, safeguarding global food security.

In conclusion, the proposed electrochemical immunosensor represents a significant step forward in the field of plant virus detection. Its ultra-low detection limit, high specificity, and practical applicability make it a powerful tool for the early and accurate detection of TBRFV, offering a promising solution for the prevention and control of viral outbreaks in agriculture. The success of this approach also opens new avenues for the development of similar biosensors for other plant.

Supplementary Information

The online version contains supplementary material available at https://doi.org/10.1186/s13007-025-01407-3.

Supplementary Material 1

Supplementary Material 2

Author contributions

N.R.: Conceptualization, Methodology, Investigation, Formal Analysis, Visualization, Writing– Original Draft.A.M.: Supervision, Conceptualization, Methodology, Writing– Review & Editing.M.R.S.: Resources, Supervision, Review & Editing. R.H.S.: Supervision, Methodology, Review & Editing.M.R.: Investigation, Investigation, Review & Editing.M.S.B.: Project Administration, Supervision, Review & Editing. All authors: Reviewed and approved the final manuscript.

Funding

This work received institutional support from Tarbiat Modares University as part of its doctoral dissertation funding program. No specific grants or financial awards were provided by external public, commercial, or non-profit funding agencies for this research.

Data availability

No datasets were generated or analysed during the current study.

Declarations

Ethics approval and consent to participate

Not applicable.

Consent for publication

Not applicable.

Competing interests

The authors declare no competing interests.

Received: 17 March 2025 / Accepted: 17 June 2025
Published online: 01 July 2025

References

1. Vásquez G, Delgado-Ortiz J, Frías-Treviño G, Aguirre-Uribe L, Flores-Olivas A. Tobamovirus fructirugosum an emerging disease: review and current situation in Mexico. Mex J Phytopathol. 2025;43(1):34.
2. Mehle N, Bačnik K, Bajde I, Brodarič J, Fox A, Gutiérrez-Aguirre I, Kitek M, Kutnjak D, Loh YL, and Maksimović Carvalho Ferreira, O. Tomato brown rugose fruit virus in aqueous environments–survival and significance of water-mediated transmission. Front Plant Sci. 2023;14:1187920.
3. Salem NM, Jewehan A, Aranda MA, Fox A. Tomato brown rugose fruit virus pandemic. Annu Rev Phytopathol. 2023;61(1):137–64.
4. Chanda B, Gilliard A, Jaiswal N, Ling K-S. Comparative analysis of host range, ability to infect tomato cultivars with Tm-22 gene, and real-time reverse transcription PCR detection of tomato brown rugose fruit virus. Plant Dis. 2021;105(11):3643–52.
5. Fidan H, Sarikaya P, Yildiz K, Topkaya B, Erkis G, Calis O. Robust molecular detection of the new tomato brown rugose fruit virus in infected tomato and pepper plants from Turkey. J Integr Agric. 2021;20(8):2170–9.
6. Panno S, Caruso AG, Barone S, Lo Bosco G, Rangel EA, Davino S. Spread of tomato brown rugose fruit virus in Sicily and evaluation of the spatiotemporal dispersion in experimental conditions. Agron. 2020;10(6):834.
7. Luria N, Smith E, Reingold V, Bekelman I, Lapidot M, Levin I, Elad N, Tam Y, Sela N, Abu-Ras A. A new Israeli tobamovirus isolate infects tomato plants harboring Tm-22 resistance genes. PLoS ONE. 2017;12(1):e0170429.
8. Avni B, Gelbart D, Sufrin-Ringwald T, Zinger A, Chen L, Machbash Z, Bekelman I, Segoli M, Dombrovsky A, Kamenetsky R. Tomato genetic resistance to tobamoviruses is compromised. Paper presented at the VI International Symposium on Tomato Diseases: Managing Tomato Diseases in the Face of Globalization and Climate Change 1316. 2019.
9. Li W, Ma C, Song Y, Hong C, Qiao X, Yin B. Sensitive detection of carcinoembryonic antigen (CEA) by a sandwich-type electrochemical immunosensor using MOF-Ce@ HA/Ag-HRP-Ab2 as a nanoprobe. Nanotechnol. 2020;31(18):185605.
10. Wang Z, Chen Z, Gao N, Ren J, Qu X. Transmutation of personal glucose meters into portable and highly sensitive microbial pathogen detection platform. Small. 2015;11(37):4970–5.
11. Lu T-C, Yang Y-J, Zhong Y, Qiu Q-Z, Chen Z-H, Chen Y-Z, Yun lei, and Ai-Lin liu. Simultaneous detection of C-reactive protein and lipopolysaccharide based on a dual-channel electrochemical biosensor for rapid Gram-typing of bacterial sepsis. Biosens Bioelectron. 2024;243:115772.
12. Zhong G-X, Ye C-L, Wei H-X, Yang L-Y, Wei Q-X, Liu Z-J, Fu L-X, Lin X-H, Chen J-Y. Ultrasensitive detection of RNA with single-base resolution by coupling electrochemical sensing strategy with chimeric DNA probe-aided ligase chain reaction. Anal Chem. 2020;93(2):911–9.
13. Han L. Current trends in electrochemical aptasensor for tumor-associated growth factor receptor detection in serum. Int J Electrochem Sci. 2022;17(6):220673.
14. Rosa BG, Akingbade OE, Guo X, Gonzalez-Macia L, Crone MA, Cameron LP, Freemont P, Choy K-L, Güder F, Yeatman E. Multiplexed immunosensors for point-of-care diagnostic applications. Biosens Bioelectron. 2022;203:114050.
15. Ying J, Lenaerts S, Symes MD, Yang XY. Hierarchical design in nanoporous metals. Adv Sci. 2022;9(27):2106117.
16. Parihar A, Choudhary N, Sharma P, Khan R. Carbon nanomaterials-based electrochemical aptasensor for point-of-care diagnostics of cancer biomarkers. Mater Today Chem. 2023;30:101499.
17. Shah N, Huang T-L, Nambiar HN, Zamborini FP. Seed-mediated electrodeposition of silver nanowires and nanorods. Langmuir. 2024;40(15):7835–42.
18. Siampour H, Abbasian S, Moshaii A, Omidfar K, Sedghi M, Naderi-Manesh H. Seed-mediated electrochemically developed Au nanostructures with boosted sensing properties: an implication for non-enzymatic glucose detection. Sci Rep. 2020;10(1):7232.
19. Mehere A, Chaure NB. Precisely controlled shape and size of gold nanostructures by seed-mediated reduction reaction method. Appl Phys A. 2020;126:1–14.
20. Hou Y-H, Wang J-J, Jiang Y-Z, Lv C, Xia L, Hong S-L, Lin M, Lin Y, Zhang Z-L, Pang D-W. A colorimetric and electrochemical immunosensor for point-of-care detection of enterovirus 71. Biosens Bioelectron. 2018;99:186–92.
21. Azri FA, Sukor R, Selamat J, Abu Bakar F, Yusof NA, Hajian R. Electrochemical immunosensor for detection of aflatoxin B1 based on indirect competitive ELISA. Toxins. 2018;10(5):196.
22. Hemben A, Ashley J, Tothill IE. Development of an immunosensor for Pf HRP 2 as a biomarker for malaria detection. Biosens. 2017;7(3):28.
23. Zhang Y, Gao Y, Zhang X, Wang H, Xia T, Bian C, Liang S, Tang X, Wang X. Electrochemical immunosensor for hbe antigen detection based on a signal amplification strategy: the co-catalysis of horseradish peroxidase and nanoporous gold. Sens Actuators B: Chem. 2019;284:296–304.
24. Ecke A, Bell J, Schneider RJ. A three-dimensional microfluidic flow cell and system integration for improved electrochemical substrate detection in HRP/TMB-based immunoassays. Sens Diagn. 2023;2(4):887–92.
25. Wignarajah S, Chianella I, Tothill IE. Development of electrochemical immunosensors for HER-1 and HER-2 analysis in serum for breast cancer patients. Biosens. 2023;13(3):355.
26. Doldán X, Fagúndez P, Cayota A, Laíz J, Tosar JP. Electrochemical sandwich immunosensor for determination of exosomes based on surface marker-mediated signal amplification. Anal Chem. 2016;88(21):10466–73.
27. Chen P, Hua X, Liu J, Liu H, Xia F, Tian D, Zhou C. A dual amplification electrochemical immunosensor based on HRP-Au@ ag NPs for carcinoembryonic antigen detection. Anal Biochem. 2019;574:23–30.
28. Martins TS, Bott-Neto JL, Oliveira Jr ON, Machado SA. A sandwich-type electrochemical immunosensor based on Au-rGO composite for CA15-3 tumor marker detection. Mikrochim Acta. 2022;189(1):38.
29. Rafidah A, Faridah S, Shahrul A, Mazidah M, Zamri I. Chronoamperometry measurement for rapid cucumber mosaic virus detection in plants. Procedia Chem. 2016;20:25–8.
30. Uda M, Hasfalina C, Samsuzanaa A, Faridah S, Zamri I, Noraini BS, Sabrina WN, Hashim U, Gopinath SC. Determination of fixed-potential selection using chronoamperometry analysis by screen-printed carbon electrode for rice tungro bacilliform virus (RTBV) detection. Paper presented at the AIP Conference Proceedings. 2017.

31. Freitas TA, Proenca CA, Baldo TA, Materon EM, Wong A, Magnani RF, Faria RC. Ultrasensitive immunoassay for detection of Citrus tristeza virus in citrus sample using disposable microfluidic electrochemical device. Talanta. 2019;205:120110.
32. Yarjoo S, Siampour H, Khalilipour M, Sajedi RH, Bagheri H, Moshaii A. Gold nanostructure-enhanced immunosensing: ultra-sensitive detection of VEGF tumor marker for early disease diagnosis. Sci Rep. 2024;14(1):10450.
33. Rezaei N, Safarnejad MR, Soheilivand S, Sajedi RH, Mahmoudian J, Shams-Bakhsh M. Development of specific polyclonal antibodies and a fluorescence-based immunoassay for detecting tomato brown rugose fruit virus-Iranian isolate. Physiol Mol Plant Pathol. 2025;138:102689. https://doi.org/10.1016/j.pmpp.2025.102689
34. Ahirwal GK, Mitra CK. Gold nanoparticles based sandwich electrochemical immunosensor. Biosens Bioelectron. 2010;25(9):2016–20.
35. Haji-Hashemi H, Habibi MM, Safarnejad MR, Norouzi P, Ganjali MR. Label-free electrochemical immunosensor based on electrodeposited Prussian blue and gold nanoparticles for sensitive detection of citrus bacterial canker disease. Sens Actuators B: Chem. 2018;275:61–8.
36. EPPO PM 7/146 (2): Tomato brown rugose fruit virus (Version 2, 2022).
37. Stanković V, Đurđić S, Ognjanović M, Antić B, Kalcher K, Mutić J, Stanković DM. Anti-human albumin monoclonal antibody immobilized on EDC-NHS functionalized carboxylic graphene/aunps composite as promising electrochemical HSA immunosensor. J Electroanal Chem. 2020;860:113928.
38. Miyake S, Irikura D, Yamasaki T. Detection of mast cells expressing c-Kit using antibody covalently bound to gelatin elongated from surface of immunosensor based on surface plasmon resonance. Anal Sci. 2019;35(7):811–3.
39. Hayashi Y, Matsuda R, Ito K, Nishimura W, Imai K, Maeda M. Detection limit estimated from slope of calibration curve: an application to competitive ELISA. Anal Sci. 2005;21(2):167–9.
40. Liu J, Liu B, Liu J, He X-D, Yuan J, Ghassemlooy Z, Torun H, Fu Y-Q, Dai X, Ng WP. Integrated label-free erbium-doped fiber laser biosensing system for detection of single cell Staphylococcus aureus. Talanta. 2023;257:124385.
41. Nourani S, Ghourchian H, Boutorabi SM. Magnetic nanoparticle-based immunosensor for electrochemical detection of hepatitis B surface antigen. Anal Biochem. 2013;441(1):1–7.
42. Gan N, Jia L, Zheng L. A sandwich electrochemical immunosensor using magnetic DNA nanoprobes for carcinoembryonic antigen. Int J Mol Sci. 2011;12(11):7410–23.
43. Shen C, Wang L, Zhang H, Liu S, Jiang J. An electrochemical sandwich immunosensor based on signal amplification technique for the determination of alpha-fetoprotein. Front Chem. 2020;8:589560.

Publisher's note